Supporting Information

A High-Spin Alkylperoxo-Iron(III) Complex with *cis*-Anionic Ligands: Implications for the Superoxide Reductase Mechanism

Tarali Devi,[ab] Kuheli Dutta,[a] Jennifer Deutscher,[a] Stefan Mebs,[c] Uwe Kuhlmann,[d] Michael Haumann,[c] Beatrice Cula,[a] Holger Dau,[c] Peter Hildebrandt,[d] and Kallol Ray[a]*

[a]*Institut für Chemie, Humboldt-Universitat zu Berlin, Brook-Taylor-Straße 2,*
12489-Berlin, Germany

[b]*Department of Inorganic and Physical Chemistry, Indian Institute of Science Bangalore,*
560012-Karnataka, India

[c]*Department of Physics, Freie Universität Berlin, Arnimallee 14, 14195 Berlin, Germany*

[d]*Institut für Chemie, Technische Universität Berlin, Fakultät II, Straße des 17. Juni 135,*
10623-Berlin, Germany

* To whom correspondence should be addressed.
E-mail: kallol.ray@chemie.hu-berlin.de

Table of Contents

Experimental Section

Materials (Chemicals and handling). The chemicals employed were purchased from the companies SIGMA-ALDRICH, ABCR, TCI and Alfa Aesar, and used without further purification. Anhydrous solvents were purchased from CARL-ROTH GmbH (acetonitrile, diethyl ether, dimethyl formamide, dichloromethane, chloroform, 1,2-dichloroethane, toluene, methanol) under the tradename ROTIDRY (>99.5%, < 50 ppm H_2O), degassed prior to use and stored over activated molecular sieves under N_2 atmosphere. Deuterated solvents were purchased from EURISOTOP. Preparation and handling of air or water-sensitive compounds were performed under an inert atmosphere using either Schlenk technique or a glovebox GS MEGA from GS-GLOVEBOX Systemtechnik GmbH filled with N_2. Nitrogen and argon of quality 5.0 were used for this purpose and were purchased from AIR LIQUIDE. Oxidants such as *t*-butylhydroperoxide (^{t}BuOOH) and cumenehydroperoxide (CumOOH) are obtained from Sigma Aldrich. ^{57}Fe complexes was synthesized following the literature procedure.[S1,S2]

Instrumentation and physical techniques.

Elemental analysis. All elemental analyses were performed by the analytical service of the Institut für Chemie of the Humboldt-Universität zu Berlin. The percentages of Carbon, Hydrogen, Nitrogen and Sulphur were determined using an HEKAtech EURO EA 3000 analyzer. The reported values are the result of an average of two independent measurements.

Nuclear magnetic resonance spectroscopy. All NMR spectra were recorded at 20 °C using a BRUKER 300 DPX spectrometer equipped with a cryostat. ^{1}H and ^{19}F NMR were recorded in deuterated solvents and chemical shifts (δ, ppm) referenced against residual protic solvent peaks.

Electrospray ionization mass spectrometry. ESI-MS spectra in solution were recorded by using an ADVION EXPRESSION CMS spectrometer; acetonitrile (HPLC grade) was used as an eluent and the sample was directly injected into the instruments. The analysis of the data was carried out with the ADVION DATA EXPRESS Version 6.0.11.3. Simulation of the isotopic pattern of the experimental base peak was performed by the use of ISOTOPE DISTRIBUTION CALCULATOR AND MASS SPEC PLOTTER software provided by SIS (Scientific Instrument Services).

Single crystal X-ray structure determinations. Data collections were performed at 100 K on a BRUKER D8 VENTURE diffractometer by using Mo Kα radiation (λ = 0.71073 Å). Multi-scan absorption corrections implemented in SADABS[S3] were applied to the data. The structures were solved by intrinsic phasing (SHELXT 2014/5)[S4] and refined by full matrix least square procedures based on F2 with all measured reflections (SHELXL-2018/3)[S5] in the graphical user interface SHELXle[S6] with anisotropic temperature factors for all non-hydrogen atoms. All hydrogen atoms were added geometrically and refined by using a riding model. Deposition number **2296883** contains the supplementary crystallographic data for this paper. These data are provided free of charge by the joint Cambridge Crystallographic Data Centre via https://www.ccdc.cam.ac.uk/structures.

X-ray absorption spectroscopy. XAS at the Fe K-edge was performed at beamline KMC-3 at the BESSY-II synchrotron (Helmholtz Center Berlin, Germany) using a set-up including a Si[111] double-crystal monochromator, a 13-element energy-resolving Si-drift detector (RaySpec) for X-ray fluorescence monitoring, and DXP-XMAP pulse-processing electronics (XIA). Samples were held at 20 K in a liquid-helium cryostat (Oxford). The energy axis of the monochromator was calibrated (accuracy ±0.1 eV) to 7112 eV using the K-edge absorption spectrum of an iron-foil (10 m). The spot size on the samples was ca. 1.5 x 3.0 mm (vertical x horizontal) as set by a focusing mirror and slits. X-ray fluorescence spectra were collected using a continuous scan mode of the monochromator (scan duration ~7 min). Up to 5 scans were averaged (2-3 scans per sample spot) for signal-to-noise ratio improvement. XAS data were processed (dead-time correction, background subtraction, normalization) to yield XANES and EXAFS spectra using our earlier described procedures and in-house software.[S7-S9] k_3 -weighted EXAFS spectra were simulated with in-house software and phase functions from FEFF9 (S_0^2 = 1.0).[S10] EXAFS simulation results are tabulated in **Table S2**.

UV–vis absorption spectroscopy experiment and data analysis. The UV–vis absorption spectra were recorded with a 8453 UV-visible Spectroscopy system from Agilent with argon purging. The measurements were carried out in 10 mm or 5 mm precision cuvettes made of SUPRASIL® quartz glass, the closures of which were equipped with a septum. The measurements at low temperatures were carried out by cooling the cuvette holder using a cooling thermostat USP-203-A from Unisoku Scientific Instruments. The analysis of the spectra was carried out with the software UV–

visible Chemstation from Agilent. For a typical UV–vis experiment, a complex solution of known concentration was prepared in the glove box and transferred into a cuvette. The cuvette was then placed in the thermostat and the measurement was started once the solution was in thermal equilibrium with the cryostat environment. A small argon stream was constantly maintained in the cuvette through the septum on top of the solution to prevent any oxygen interferences with the monitored reactions when required. The solutions of the different reactants were prepared in a minimum amount of solvent and then injected into the cuvette through the septum using air-tight syringes. The changes in the UV–vis spectra were then recorded. The reported molar extinction coefficients (ε) of the specific absorption maxima ($\lambda_{\max}$) are mean values of several individual measurements.

Gas Chromatography (GC). GC analysis was carried out by using an AGILENT 7890B gas chromatograph (HP5 column, 30 m) with a flame-ionization detector. GC-MS was performed on an AGILENT 5977B spectrometer with a triple-axis detector.

Resonance Raman (rRaman). Resonance Raman spectra were measured in both CH_3CN and CD_3CN at -40 °C (Bruker cryostat) with 406 nm and 514 nm excitation form Kr^+ and Ar^+-laser (Coherent) respectively at 1 mW power employing a Horiba Jobin-Yvon LabRAM HR800 confocal Raman spectrometer. The sample concentrations were 4 mM.

Electron paramagnetic resonance (EPR). X-band CW EPR spectra used for qualitative analysis of **2** was collected by a Bruker EMXplus Instrument at a ca. 9.35 GHz (X-Band) frequency in perpendicular mode. All samples measured for qualitative analysis were measured at an average temperature of 13 K as frozen solutions by the use of a liquid helium recirculating cooling system provided by ColdEdge.

Computational Methodology. Structurally relaxed molecular models of **2**, **3**-Cl, **5** and non-coordinated ^{t}BuOOH with $[Fe^{III}(12\text{-TMC})(OH)]^{2+}$ were obtained by DFT optimizations at the UB3PW91/6-311+G(2df,p)[S11] level of theory applying Gaussian16.[S12] For the iron atoms an effective core potential was employed.[S13] The COSMO solvation model was used to mimic the acetonitrile solvation.[S14] Dispersion was taken in account by the empirical dispersion correction of Grimme.[S15] Subsequent normal mode analysis (frequency calculation) proved all structures to be minima on the potential energy hypersurface.

Syntheses

1. Synthesis of ligand

(a) 12-TMCO (4,7,10-trimethyl-1-oxa-4,7,10-triazacyclotedodecane) synthesis

Synthesis of the TMCO ligands were synthesized by slight modifications of the previously reported synthetic pathways.[S16–S18]

Synthesis of *N,N',N"*-tritosylbis(2-aminoethyl)amine

This synthesis was performed with small modifications on a previously reported procedure.[S17] 2,2'-diaminodiethylamine (3.28 g, 25 mmol) and NaOH (3.6 g, 90 mmol) were dissolved in 20 mL H_2O inside a three-necked round bottom flask placed in a water bath. The reaction mixture was stirred for some minutes until the NaOH was completely dissolved. A solution of *p*-toluensulfonyl chloride (14.6 g, 76 mmol) in diethylether was then added dropwise with vigorous stirring over 1 hour. The resultant reaction mixture was stirred at room temperature for 2 more hours and left standing overnight when two layers were formed. The diethylether layer was separated from the aqueous one, washed with H_2O (3 x 20 mL) and dried over $MgSO_4$. The solvent was removed and the resulting solid was dried under vacuum. *N,N',N"*-tritosylbis(2-aminoethyl)amine was collected as a colourless glassy solid. Yield: 13.12 g (22.5 mmol, 90%). ^1H NMR ($CDCl_3$, 400 MHz): δ [ppm] ($CDCl_3$, 300 MHz): δ [ppm] = 7.79 (d, 2H, Ar-H), 7.69 (d, 4H, Ar-H), 7.29-7.26 (m, 2H, Ar-H), 7.23-7.19 (m, 4H, Ar-H), 3.41 (dd, 4H, N-CH_2), 2.88 (m, 4H, N-CH_2), 2.54 (t, 3H, CH_3), 2.36 (t, 6H, CH_3) (**Fig. S14**).

Synthesis of 4,7,10-Tritosyl-1-oxa-4,7,10-triazacyclododecane

This synthesis was performed making small modifications to a previously reported procedure.[S18,S19] Under N_2 atmosphere, *N,N',N"*-tritosylbis(2-aminoethyl)-amine (2.28 g, 4 mmol) and Cs_2CO_3 (3.28 g, 10 mmol) were mixed in 60 mL of dimethylformamide (DMF). A white suspension was formed and it was stirred for an hour. A solution of diethyleneglycol-ditosylate (1.67 g, 4 mmol) in 20 mL of DMF was then added dropwise over 5 hours. The cloudy white solution was stirred for 3 days in an inert atmosphere. After this time, the reaction mixture was opened to air, and ice (around 50 mL) was added slowly while stirring. Once the ice was almost fully melted, the reaction mixture was left in the fridge overnight. The white precipitate thus formed, was filtered and dried under vacuum. The protected macrocycle 4,7,10-tritosyl-1-oxa-4,7,10-triazacyclododecane, was obtained as a white solid. Yield: 2.44 g (3.7 mmol, 92%). ^{1}H NMR ($CDCl_3$, 400 MHz): δ [ppm] = ^{1}H NMR ($CDCl_3$, 300 MHz): δ [ppm] = 7.82 (d, 2H, H-Ar), 7.63 (d, 4H, H-Ar), 7.35 (d, 2H, H-Ar), 7.31 (d, 4H, H-Ar), 3.66 (t, 4H, O-CH_2), 3.52 (d, 4H, O-CH_2-CH_2), 3.22-3.17 (m, 8H, N-CH_2-CH_2-N), 2.46 (s, 3H, N-CH_3), 2.43 (s, 6H, N-CH_3) (**Fig. S15**).

Synthesis of 1-oxa-4,7,10-triazacyclododecane

This synthesis was performed by making small modifications to a previously reported procedure.[S18] 4,7,10-tritosyl-1-oxa-4,7,10-triazacyclotetradecane (2.44 g, 3.7 mmol) and HBr 30% in acetic acid (70 mL) were refluxed under inert conditions for 48 hrs. After this time, a white precipitate was formed. It was filtered with a small pore frit, washed with cold acetone and dried under vacuum. The HBr salt of 1-oxa-4,7,10-triazacyclotetradecane was obtained as a white powder. Yield: 1.00 g (2.3 mmol, 63 %). ^{1}H NMR (D_2O, 300 MHz): δ [ppm] = 3.81 (t, 4H, O-CH_2-CH_2), 3.33 (t, 4H, O-CH_2-CH_2), 3.22 (t, 4H, N-CH_2-CH_2), 3.06 (t, 4H, N-CH_2-CH_2) (**Fig. S16**).

Synthesis of 4,7,10-trimethyl-1-oxa-4,7,10-triazacycloteddodecane (12-TMCO)

This synthesis was performed by making small modifications to a previously reported procedure.[S19] The HBr salt of 1-oxa-4,7,10-triazacyclotetradecane (0.95 g, 4.5 mmol) was refluxed with formic acid (4.8 mL), formaldehyde (4 mL) and water (0.5 mL) for 24 hrs. After this time, the clear solution was transferred to a beaker, put in an ice bath, and treated with NaOH (7.5 M) until pH > 12.0. The reaction mixture was then extracted with chloroform (5 x 10 mL). The organic phase was dried with Na_2SO_4 and the solvent was removed. The 12-TMCO ligand was obtained as a yellow oil. Yield: 530 mg (2.2 mmol, 50%). ^{1}H NMR ($CDCl_3$, 300 MHz): δ [ppm] = 1H NMR ($CDCl_3$, 300 MHz): δ [ppm] = 3.54 (m, 4H, O-CH_2-CH_2), 2.55 (m, 8H, N-CH_2-CH_2-N), 2.53 (m, 4H, O-CH_2-CH_2), 2.23 (s, 3H, N-CH_3), 2.22 (s, 6H, N-CH_3) (**Fig. S17**).

(b) 12-TMC (1,4,7,10-tetramethyl-1,4,7,10-tetraazacyclododecane) synthesis

The 12-TMC ligand was synthesized following previously reported the literature procedures. *N*-Methylation of 12-Cyclen was accomplished by refluxing cyclen (1.00 g, 5.8 mmol), 5.3 mL formic acid (98-100 %), 4.4 mL formaldehyde (37 %) in 10 mL water for 12 hr. The reaction mixture was then transferred with 25 mL water to a beaker and cooled in an ice bath. A concentrated aqueous solution of KOH (15 g in 50 mL) was added slowly. The product was extracted with chloroform, dried over $MgSO_4$, filtered, and the solvent removed under vacuum which resulted ~70-75% isolated yield of 12-TMC. ^1H NMR (300 MHz, $CDCl_3$): δ [ppm] = 2.47 (s, 16H, N-CH_2-CH_2-N), 2.17 (s, 12H, N-CH_3) (**Fig. S18**).

2. Synthesis of Fe-complexes

(a) Synthesis of complex [Fe^{II}(12-TMCO)(OTf)$_2$], 1-(OTf)$_2$

The 12-TMCO ligand (30 mg, 0.14 mmol, 1.0 equiv.) was suspended in 1.5 mL acetonitrile at room temperature inside the glovebox. To this, a solution of $Fe(OTf)_2(CH_3CN)_2$ (64 mg, 0.14 mmol, 1.0 equiv.) in 1.5 mL acetonitrile was added dropwise under continuous stirring. This solution was left to stir for 3 days. The solution was then filtered using a syringe filter. To the filtrate, about 15 mL of diethylether was added which resulted in a white cloudy precipitate. When this cloudy precipitate was allowed to stand at -30°C overnight, pale white crystals appeared. The solvent was decanted from the top and the residue was dried completely under Schlenck line to afford the final complex (60 mg, 66%). ^1H NMR (300 MHz, CD_3CN) due to paramagnetic broadening of signals, it was not possible to assign the peaks unequivocally (**Fig. S2**). ^{19}F NMR (300 MHz, CD_3CN) chemical shift value (δ) -79 ppm (s) indicates free triflate in solution (**Fig. S2a**). ESI-MS: [Fe^{II}(12-TMCO)(OTf)]$^+$; m/*z* = 420.0 (experimental), 420.0 m/*z* (calculated). Elemental analysis: C19H40F6FeN4O9S2 C, 32.49; H, 5.17; N, 5.16 (experimental), C, 39.09; H, 2.18; N, 10.31; (calculated).

(b) Synthesis of complex 1-Cl

The 12-TMCO ligand (30 mg, 0.14 mmol, 1.0 equiv.) was suspended in 1.5 mL acetonitrile at room temperature inside the glovebox. To this, a solution of $FeClBF_4$ (25 mg, 0.14 mmol, 1.0 equiv.) in 1.5 mL acetonitrile was added dropwise under continuous stirring. This solution was left to stir for 3 days. The solution was then filtered using a syringe filter. About 15 mL of diethylether was added to the filtrate, resulting in a white cloudy precipitate that was allowed to stand at -30°C overnight for the ppt to settle down. The solvent was decanted from the top and the residue was dried completely under Schlenck line to afford the final complex (35 mg, 64%). The product was characterized by ESI-MS spectroscopy. ESI-MS: $[Fe^{II}(12\text{-}TMCO)(Cl)]^+$; m/*z* = 306.1 (experimental), m/*z* = 306.1 (calculated).

(c) Synthesis of complex $[Fe^{II}(12\text{-}TMC)(CH_3CN)_2]^{2+}$, 8

The 12-TMC ligand (30 mg, 0.14 mmol, 1.0 equiv.) was dissolved in 1.5 mL acetonitrile at room temperature inside the glovebox. To this, a solution of $Fe(OTf)_2(CH_3CN)_2$ (64 mg, 0.14 mmol, 1.0 equiv.) in 1.5 mL acetonitrile was added dropwise under continuous stirring. The resulting solution turned beige and was allowed to run overnight. The solution was then filtered using a syringe filter. To the filtrate, about 15 mL of diethylether (Et_2O) was added which resulted in a brown oil to form. This oil was washed 3 times with more diethylether that resulted beige coloured fine solids. Removal of Et_2O and drying the product under vacuum yield the corresponding $[Fe^{II}(12\text{-}TMC)]^{2+}$ complex (72 mg, 86%). Elemental analysis: $C_{14}H_{28}F_6FeN_4O_6S_2$ C, 28.60; H, 4.56; N, 8.91 (experimental), C, 28.87; H, 4.85; N, 8.62; (calculated). ESI-MS: m/*z* = 319.0 for $[Fe^{II}(12\text{-}TMC)Cl]^+$ (under mass condition) (experimental); m/*z* = 319.14 (calculated).

3. Synthesis of ^{57}Fe enriched metal complexes for Mössbauer studies

An ^{57}Fe-enriched **1**-$(OTf)_2$ (^{57}**1**-$(OTf)_2$) was necessary for performing Mössbauer studies in solution. In order to synthesize ^{57}**1**-$(OTf)_2$, $^{57}Fe(OTf)_2(CH_3CN)_2$ was generated first. In an inert atmosphere, metallic ^{57}Fe (42 mg, 0.74 30 mmol) and a degassed concentrated HCl solution (4 mL) were stirred at 65°C overnight until all the iron was dissolved. The solvent was then removed by vacuum and the resultant white residue ($^{57}FeCl_2$) was suspended in dry CH_3CN (4 mL). $(CH_3)_3Si(OTf)$ (820 mg, 3.69 mmol) in dry CH_3CN (2 mL) was added dropwise over 2 minutes. The resultant solution was stirred overnight and then the solvent was removed by vacuum. The remaining solid was re-dissolved in a minimum amount of dry CH_3CN and an excess of dry Et_2O was added. The mixture was left overnight at -20°C during which time white crystals were formed. The crystals were filtered, washed with dry Et_2O and dried. $^{57}Fe(OTf)_2(CH_3CN)_2$ was obtained as a white solid. Yield: 175 mg (0.4 mmol, 55%). This product was directly employed in the synthesis of ^{57}**1**-$(OTf)_2$; the procedure described for the synthesis of **1**-$(OTf)_2$ was followed, this time using $^{57}Fe(OTf)_2(CH_3CN)_2$ instead of $Fe(OTf)_2(CH_3CN)_2$.

4. Generation of the intermediates and sample preparations

(a) Generation of intermediate 2

Under inert condition, a solution of complex **1** (0.5 mM, 0.9 mL) was prepared in acetonitrile in a quartz cuvette. The cuvette was cooled to -20°C. To this solution, 20 equiv. ^{t}BuOOH (in CH_3CN; 0.1 mL) was added. The formation of the resultant intermediate was followed by monitoring the bands at 770 nm (ε = 142 M^{-1} cm^{-1}) and 935 nm (ε = 170 M^{-1} cm^{-1}) via UV-vis spectroscopy. For spectroscopic studies the intermediate was generated in higher concentrations (XAS = 4 mM, rR = 4 mM).

(b) Generation of intermediate 3-Cl

The intermediate **3**-Cl was generated in three different ways:

In the first experiment under inert condition, a solution of complex **1-**$(CH_3CN)_2$ (0.5 mM, 0.9 mL) was prepared in CH_3CN in a quartz cuvette and lowered its temperature to -20 °C. Then, consecutive addition of 5 equiv. tetraethylammonium chloride (NEt_4Cl) and 20 equiv. ^{t}BuOOH in CH_3CN to **1** at -20 °C resulted the generation of λ_{max} = 517 nm peak monitored through UV-vis spectroscopy (ε = 880 M^{-1} cm^{-1}). For spectroscopic studies the intermediate was generated in higher concentrations (XAS = 4 mM, rR = 4 mM, EPR = 1 mM). In the second method **3**-Cl was generated from species **2** after addition of 5 equiv. NEt_4Cl to its acetonitrile in the presence of ^{t}BuOOH solution at -20 °C. The UV-vis spectral changes due to the concomitant decay of **2** at λ_{max} = 770 nm, 935 nm and the formation of **3**-Cl at λ_{max} = 517 nm was monitored by UV-vis spectroscopic technique.

References

(S1) X. Engelmann, D. D., Malik, T., Corona, K. Warm, E. R. Farquhar, M. Swart, W. Nam, K. Ray, *Angew. Chem. Int. Ed.* 2019, **58**, 4012.

(S2) K. Warm, A. Paskin, U. Kuhlmann, E. Bill, M. Swart, M. Haumann, H. Dau, P. Hildebrandt, K. Ray, *Angew. Chem. Int. Ed.* 2021, **60**, 6752.

(S3) G. M. Sheldrick, *SADABS, Empirical Absorption Correction Program*, University of Göttingen, Germany, 2002.

(S4) G. M. Sheldrick, *Acta Crystallogr. Sect. A* 2015, **71**, 3.

(S5) G. M. Sheldrick, *Acta Crystallogr. Sect. C* 2015, **71**, 3.

(S6) C. B. Hübschle, G. M. Sheldrick, B. Dittrich, *J. Appl. Crystallogr.* 2011, **44**, 1281.

(S7) N. Schuth, S. Mebs, D. Huwald, P. Wrzolek, M. Schwalbe, A. Hemschemeier, M. Haumann, *Proc. Natl. Acad. Sci.* 2017, **114**, 8556.

(S8) H. Dau, P. Liebisch, M. Haumann, *Anal. Bioanal. Chem*. 2003, **376**, 562.

(S9) S. Yao, V. Forstner, P. W. Menezes, C. Panda, S. Mebs, E. M. Zolnhofer, M. E. Miehlich, T. Szilvási, N. A. Kumar, M. Haumann, K. Meyer, H. Grützmacher, M. Driess, *Chem. Sci*. 2018, **9**, 8590.

(S10) J. J. Rehr, J. J. Kas, F. D. Vila, M. P. Prange, K. Jorissen, *Phys. Chem. Chem. Phys.* 2010, **12**, 5503.

(S11) a) A. D. Becke, *J. Chem. Phys*. 1993, **98**, 5648. b) J. P. Perdew, J. A. Chevary, S. H. Vosko, K. A. Jackson, M. R. Pederson, D. J. Singh, C. Fiolhais, *Phys. Rev. B* 1992, **46**, 6671.

(S12) M. J. Frisch, G. W. Trucks, H. B. Schlegel, *Gaussian 16, Revision C.01*, Gaussian, Inc., Wallingford CT, 2016.

(S13) a) M. Dolg, U. Wedig, H. Stoll, H. Preuss, *J. Chem. Phys*. 1987, **86**, 866. b) J. M. L. Martin, A. Sundermann, *J. Chem. Phys*. 2001, **114**, 3408.

(S14) A. Klamt, G. Schürmann, *J. Chem. Soc. Perkin Trans.* 1993, **2**, 799.

(S15) S. Grimme, J. Antony, S. Ehrlich, H. Krieg, *J. Chem. Phys*. 2010, **132**, 154104.

(S16) M. T. S. Amorim, S. Chaves, R. Delgado, J. J. R. Fraústo DaSilva, *J. Chem. Soc. Dalton Trans.* 1991, **10***,* 3065.

(S17) T. W. Bell, H. J. Choi, W. Harte, M. G. B. Drew, *J. Am. Chem. Soc.* 2003, **125**, 12196.

(S18) C. S. Rossiter, R. A. Mathews, J. R. Morrow, *Inorg. Chem.* 2005, **44**, 9397.

(S19) J. M. Wilson, F. Giordani, L. J. Farrugia, M. P. Barrett, D. J. Robins, A. Sutherland, *Org. Biomol. Chem.* **2007**, *5*, 3651.

(S20) Y. Zang, J. Kim, Y. Dong, E. C. Wilkinson, E. H. Appelman, L. Que Jr., *J. Am. Chem. Soc.* 1997, **119**, 4197.

(S21) M. R. Bukowski, H. L. Halfen, T. A. van den Berg, J. A. Halfen, L. Que Jr. *Angew. Chem. Int. Ed.* 2005, **44**, 584.

(S22) F. Namuswe, T. Hayashi, Y. Jiang, G. D. Kasper, A. A. N. Sarjeant, P. Moënne-Loccoz, D. P. Goldberg, *J. Am. Chem. Soc*. 2010, **132**, 157.

(S23) S. Hong, Y.-M. Lee, K.-B. Cho, M. S. Seo, D. Song, J. Y. R. Garcia- Serres, M. Clémancey, T. Ogura, W. Shin, J.-M. Latour, W. Nam, *Chem. Sci.* 2014, **5**, 156.

(S24) N. Lehnert, R. Y. N. Ho, L. Que, Jr., E. I. Solomon, *J. Am. Chem. Soc.* 2001, **123**, 8271.

(S25) T.-C. Yang, R. L. Mc Naughton, M. D. Clay, F. E. Jenney Jr., R. Krishnan, D. M. Kurtz Jr., M. W. W. Adams, M. K. Johnson, B. M. Hoffman, *J. Am. Chem. Soc.* 2006, **128**, 16566.

(S26) L. R. Widger, Y. Jiang, A. C. Mc Quilken, T. Yang, M. A. Siegler, H. Matsumura, P. Moënne-Loccoz, D. Kumar, S. P. de Visser, D. P. Goldberg, *Dalton Trans.* 2014, **43**, 7522.

Table S1a. Selected bond lengths and angles of **1-**(OTf)$_2$

Atoms	***d* [Å]**	**Atoms**	**Angles [°]**
Fe-N1	2.215(3)	O $^{(Triflate)}$-Fe-O $^{(Ligand)}$	166.67(9), 85.4(8)
Fe-N2	2.223(3)		
Fe-N3	2.196(3)		
Fe-O $^{(Ligand)}$	2.167(2)		
Fe-O $^{(Triflate)}$	2.131(2)		
	2.045(2)		

Table S1b. Crystallographic table for **1**-(OTf)$_2$

Space group	**P*bcn***
Unit cell parameters	a = 35.662(2) b = 8.8757(6) c = 15.3809(9) α = 90° β = 90° γ = 90° *V* = 4868.5(5)
Z	8
Temperature	100(2) K
Total number of reflections collected ($I > 2\sigma(I)$)	7055
μ (mm^{-1})	0.87
Θ_{min}, Θ_{max}	2.36, 25.33
F (000)	2336
Crystal dimensions [mm X mm X mm]	0.23 × 0.07 × 0.07
h, k, l range	$-42 < h < 42$ $-10 < k < 10$ $-18 < l < 17$
R factor	0.042
wR factor	0.090
Goodness of Fit (GooF)	1.017

Table S2. EXAFS simulation parameters for complexes **1**-$(CH_3CN)_2$, **1**-Cl, **2**, and **3**-Cl

Species	**Shell**	**N [per Fe]**	**R [Å]**	**$2\sigma^2$x10^{-3} [$Å^2$]**	**R_F (1-3.5 Å)**
1-$(CH_3CN)_2$	Fe-N	3[a]	2.14	5[d]	19.1 %
	Fe-O	1[a]	2.05	5[d]	
	Fe--C	6.3[b]	2.94	9[e]	
	Fe--C	4.7[b]	3.59	9[e]	
	Fe-N	1.8[c]	2.26	2[a]	
	Fe--C	1.8[c]	3.08	2[a]	
1-Cl	Fe-N	3[a]	2.14	10[d]	18.4%
	Fe-O	1[a]	2.04	10[d]	
	Fe--C	5.0[b]	2.98	9[e]	
	Fe--C	6.0[b]	3.52	9[e]	
	Fe-Cl	0.8	2.32	2[a]	
2	Fe-N	3[a]	2.05	3[d]	19.8%
	Fe-O	1[a]	1.90	3[d]	
	Fe--C	5.2[b]	2.92	11[e]	
	Fe--C	5.8[b]	3.57	11[e]	
	Fe-O	0.7	1.64	2[a]	
	Fe-N	0.7[c]	2.22	2[a]	
	Fe-C	0.7[c]	3.00	2[a]	
3-Cl	Fe-N	3[a]	2.19	3[d]	17.3%
	Fe-O	1[a]	2.04	3[d]	
	Fe--C	4.3[b]	2.98	10[e]	
	Fe--C	6.7[b]	3.62	10[e]	
	Fe-O	0.8	1.82	2[a]	
	Fe--O	0.8	3.15	2[a]	
	Fe-Cl	1.2	2.26	2[a]	

N, coordination number; R, interatomic distance; $2\sigma^2$, Debye-Waller factor; R_F, fit error sum; [a] Fixed parameters; [b] coupled to a sum of 11; [c] coupled to the same value; [d, e] coupled to yield the same σ-values**.**

Table S3a. DFT coordinates of **2**

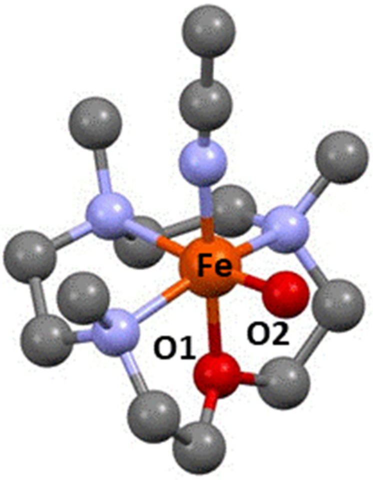

Fe	0.01032600	-0.02358200	-0.42008400
N	-0.36865200	1.98182600	-0.22821800
N	0.31381900	0.08177600	1.72374300
N	-0.28662900	-2.00410600	-0.07644100
O	-1.94348800	-0.11249900	-0.32730000
C	-2.65465300	1.12717700	-0.55227300
C	-1.63257300	2.14199700	-0.99960800
C	-0.58071400	2.29785500	1.22803100
C	-0.74815400	1.04896600	2.08015500
C	0.09733000	-1.28357200	2.26650500
C	-0.75563700	-2.11452100	1.34108000
C	-1.40353500	-2.34935500	-0.99176600
C	-2.51964800	-1.31649900	-0.88409200
H	-3.41120600	0.97974400	-1.32190600
H	-3.15332300	1.39563300	0.38003600
H	-1.38730400	1.99095400	-2.04911800
H	-2.02087000	3.15626700	-0.86943600
H	0.28206900	2.86810800	1.56602100
H	-1.44841700	2.95148900	1.33871200
H	-0.68359700	1.32394700	3.13846400
H	-1.71586100	0.57655900	1.92624000
H	1.07837100	-1.74228500	2.38459500
H	-0.35629400	-1.24483700	3.26141000
H	-0.73677200	-3.16419300	1.64643300
H	-1.79138100	-1.78564300	1.38366400
H	-0.99657600	-2.36504600	-1.99997200
H	-1.78293100	-3.34650300	-0.75024700
H	-2.92787000	-1.09621400	-1.87064000
H	-3.33008200	-1.62694100	-0.22296500
C	0.64758600	2.88236700	-0.81198700
H	0.79790500	2.61733900	-1.85685400
H	0.31054200	3.92025000	-0.74181300
H	1.58695400	2.77665200	-0.27419800

C	1.60885200	0.57950300	2.24165100
H	1.54496100	0.70300000	3.32720700
H	2.39850000	-0.13138400	2.01578300
H	1.86928000	1.53541100	1.79556200
C	0.85711800	-2.89804400	-0.34144300
H	0.54500800	-3.93952500	-0.22698000
H	1.20933100	-2.73419400	-1.35797800
H	1.66542300	-2.69189300	0.35595700
O	-0.04788000	-0.07012900	-2.03251100
N	1.92995500	-0.00023600	-0.55554400
C	3.04955400	0.00035400	-0.79215300
C	4.45951700	0.00368900	-1.07865900
H	4.83283100	-1.02168600	-1.07899400
H	4.62909600	0.45263000	-2.05871600
H	4.98499300	0.58218700	-0.31701800

Table S3b. DFT coordinates of **3-**Cl

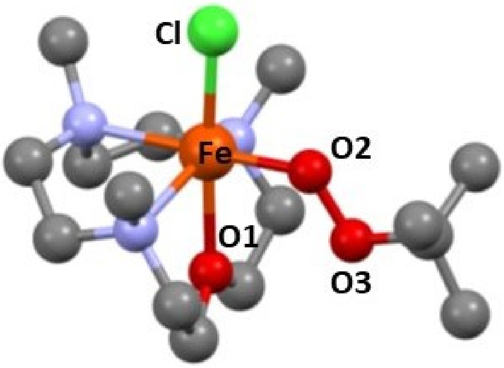

Fe	0.42259600	-0.01321900	-0.45899900
N	0.71977400	2.07931300	0.27598100
N	2.69784200	0.03402600	-0.17207500
N	0.75798000	-2.07727800	0.31056500
O	-0.00387900	-0.02859000	1.70202300
C	-0.15294500	1.19054200	2.41593400
C	-0.26388400	2.27128700	1.36537800
C	2.12117600	2.24860900	0.75119100
C	2.83718300	0.92660800	0.99284000
C	3.12112400	-1.35190300	0.11385400
C	2.10226700	-2.11708600	0.92926900
C	-0.29893200	-2.32572900	1.31374500
C	-0.31962100	-1.23944600	2.37388500
H	-1.06411200	1.16688100	3.01901900
H	0.70092200	1.33028500	3.08734300
H	-1.25516500	2.22221300	0.91535000
H	-0.13828800	3.25880200	1.82426900
H	2.65948300	2.82772500	0.00188000
H	2.13893200	2.84355100	1.66895600
H	3.89541400	1.13037300	1.20071700
H	2.42892800	0.42229800	1.86687100
H	3.27128200	-1.84196400	-0.84921100
H	4.08777900	-1.36717800	0.63245800
H	2.43431500	-3.15487400	1.04538000
H	2.03449300	-1.69732800	1.93141500
H	-1.24885100	-2.32950500	0.77977700
H	-0.16515100	-3.30605700	1.78570900
H	-1.31607600	-1.17300200	2.81788200
H	0.40341800	-1.41154600	3.17761500
C	0.41706500	3.04074900	-0.80272100
H	-0.60586900	2.88786600	-1.14468900
H	0.52662500	4.07125200	-0.44750500
H	1.09162600	2.87819200	-1.64177800
C	3.51103200	0.54115700	-1.29158600
H	4.56672600	0.59334600	-0.99943600
H	3.40284700	-0.12082200	-2.14682100

H	3.18086100	1.53160900	-1.59585700
C	0.64129400	-3.06882900	-0.77281900
H	0.75340300	-4.08418600	-0.37644100
H	-0.33545000	-2.97377300	-1.24562700
H	1.40535200	-2.89252600	-1.52733800
O	-1.44772600	-0.01886300	-0.72222900
O	-2.39617000	0.01919200	0.29574000
C	-3.73739300	0.01373000	-0.27073000
C	-3.96142400	-1.27134600	-1.05413700
C	-3.93547000	1.24659100	-1.14036900
C	-4.61218800	0.06532700	0.97329900
H	-4.98548200	-1.30163700	-1.43274900
H	-3.27989100	-1.32992200	-1.90356100
H	-3.80711600	-2.14498800	-0.41664200
H	-4.96030500	1.27430900	-1.51706100
H	-3.75803900	2.15820800	-0.56510300
H	-3.25662700	1.23084200	-1.99378800
H	-5.66364200	0.06442500	0.67994500
H	-4.43438000	-0.80254500	1.61191500
H	-4.41833700	0.97244200	1.54966300
Cl	0.67413000	-0.09629200	-2.72625600

Table S3c. DFT coordinates of **5**

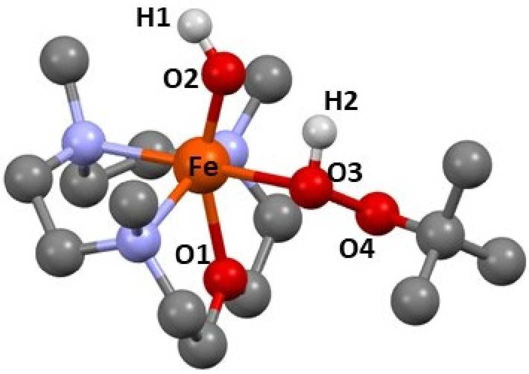

Fe	-0.57573300	-0.00289100	-0.50337100
N	-1.07789600	-2.08782400	0.11547200
N	-2.75684700	0.15151700	-0.45066600
N	-0.73437400	2.07186300	0.20692900
O	-0.02243700	-0.08574300	1.53013600
C	-0.15086600	-1.30396900	2.26970500
C	-0.16028600	-2.40301700	1.23978900
C	-2.51455000	-2.11599100	0.51640000
C	-3.09716800	-0.72399100	0.69532100
C	-3.11696300	1.56869600	-0.19580200
C	-2.11766200	2.24270500	0.71435200
C	0.25651900	2.24400000	1.29503800
C	0.17389900	1.10962200	2.29282800
C	-0.82044500	-3.05006200	-0.97909500
C	-3.43751000	-0.30172300	-1.68107900
C	-0.43928200	3.02809500	-0.88125000
H	0.70405400	-1.42067700	2.93873500
H	-1.06313600	-1.26526900	2.87222100
H	0.84124300	-2.50122600	0.81826100
H	-0.43555100	-3.35645800	1.70124900
H	-3.06617700	-2.65821000	-0.25036000
H	-2.63726400	-2.68138800	1.44331000
H	-4.18469700	-0.79548300	0.80421700
H	-2.71530200	-0.25835100	1.60317900
H	-3.14907100	2.07095300	-1.16241900
H	-4.12161200	1.63294600	0.23358800
H	-2.35611800	3.30728800	0.80292700
H	-2.17314700	1.82580300	1.71902800
H	1.24123800	2.26021200	0.83189100
H	0.10525000	3.20073700	1.80519400
H	1.10428600	1.03358900	2.85917900
H	-0.65092800	1.21759300	3.00216400
H	0.22423100	-2.98628500	-1.27761100
H	-1.44561400	-2.81523200	-1.83792900
H	-1.03798600	-4.06947800	-0.64644900
H	-3.19130300	0.36968100	-2.50131900

H	-4.52171100	-0.29257700	-1.53250000
H	-3.13185300	-1.31018500	-1.94754700
H	0.56461200	2.84360700	-1.25962200
H	-0.50107500	4.05418300	-0.50638100
H	-1.14737000	2.90203100	-1.69745200
O	1.71473200	0.44614800	-0.79754000
O	2.56316300	-0.52381900	-0.16391400
C	3.96074100	-0.11784000	-0.24341200
C	4.17080100	1.20620600	0.47174900
C	4.40629300	-0.05992500	-1.69682600
C	4.63238200	-1.26650500	0.49781800
H	5.23419200	1.45433500	0.47968000
H	3.64398800	2.01577000	-0.03563200
H	3.82640600	1.14748300	1.50612800
H	5.48235900	0.11758800	-1.74495300
H	4.19342100	-1.00276400	-2.20594300
H	3.91828900	0.75580800	-2.23505600
H	5.70959000	-1.09334800	0.52301300
H	4.27084600	-1.33181800	1.52573300
H	4.44877900	-2.21806000	-0.00460100
H	1.67348200	0.15438700	-1.72729000
O	-0.28725100	-0.01456200	-2.29332200
H	-0.92454100	-0.09492000	-3.00722500

Table S3d: DFT coordinates corresponding to **Figure S13 (b)**

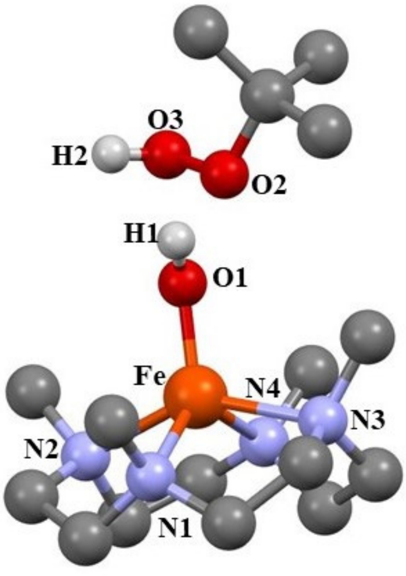

Fe	0.92425000	-0.07493500	-0.24626600
N	0.31632900	1.52230400	1.13407600
N	2.30978100	1.46831900	-0.88708000
N	2.55226000	-1.38780200	-0.84667700
N	1.05476500	-1.24225700	1.59517300
C	1.10017200	-0.24751300	2.69724100
C	0.11203800	0.87038300	2.45610300
C	1.37482400	2.58007100	1.14043800
C	2.63038300	2.19896400	0.36219800
C	3.51670800	0.80124600	-1.44522200
C	3.77158200	-0.54528100	-0.79606900
C	2.58806600	-2.50867600	0.12519100
C	2.30664400	-2.04092900	1.53722600
H	0.88931200	-0.73105600	3.65647600
H	2.11545400	0.14845200	2.75252600
H	-0.90597000	0.48141500	2.47031700
H	0.18122900	1.60945100	3.25934100
H	0.93714500	3.48440800	0.71926600
H	1.65738200	2.82015700	2.16718800
H	3.20304600	3.10311700	0.13036700
H	3.27876900	1.56067200	0.96276100
H	3.35396000	0.68181100	-2.51572100
H	4.39247000	1.44585100	-1.32667100
H	4.60075600	-1.04764200	-1.30482900
H	4.06792000	-0.42216800	0.24590200
H	1.83227000	-3.22759600	-0.19356900
H	3.55540600	-3.01984800	0.08620200
H	2.23544300	-2.90557400	2.20347200
H	3.12343400	-1.42409600	1.91167600
C	-0.97547700	2.10722300	0.69742700
H	-1.72638900	1.32340800	0.61994100

H	-1.30817800	2.86118000	1.41729200
H	-0.86344600	2.57386600	-0.27857300
C	1.73763000	2.38093100	-1.89985000
H	2.48866900	3.11500900	-2.20698200
H	1.41061400	1.80908800	-2.76588300
H	0.88120600	2.91205300	-1.49198600
C	2.35304600	-1.93662200	-2.20694900
H	3.16848600	-2.62333700	-2.45434200
H	1.40433900	-2.46770000	-2.24695100
H	2.33046100	-1.13677100	-2.94329200
C	-0.12037400	-2.13424100	1.71889000
H	-0.12801100	-2.84823800	0.89672400
H	-0.07686700	-2.67688400	2.66761500
H	-1.04225400	-1.55741200	1.67656700
O	-3.02194900	-1.05553200	-1.26544400
O	-3.58020100	-0.53217000	-0.05230500
C	-4.92729900	-0.04051000	-0.29036000
C	-5.83288700	-1.17914300	-0.73551000
C	-4.89827900	1.09194700	-1.30535000
C	-5.31227500	0.46199600	1.09476300
H	-6.86315300	-0.82502500	-0.80986500
H	-5.54087800	-1.55709500	-1.71710000
H	-5.80541000	-2.00037300	-0.01536800
H	-5.90327100	1.49896100	-1.43628200
H	-4.24314300	1.89752700	-0.96713900
H	-4.54788700	0.73682700	-2.27555200
H	-6.32014100	0.87943900	1.05933600
H	-5.30276200	-0.35162700	1.82292400
H	-4.62927200	1.24494000	1.43008900
H	-3.12835400	-2.01078400	-1.14687900
O	-0.36056200	-0.23050900	-1.45504500
H	-1.28014800	-0.54342300	-1.34317700

Table S4. Comparison of important bond distances as determined experimentally by Fe K-edge EXAFS and theoretically from DFT of **2**

Bond	**Distance from EXAFS (Å)**	**Distance from DFT (Å)**
Fe-O (oxo)	1.64	1.60
Fe-O (ligand)	1.90	2.07
Fe-N (avg)	2.05	2.04

Table S5. Comparison of different rRaman stretching frequencies (Fe-O, O-O) in different HS and LS iron(III)alkylperoxo species

Complex^a	Spin state	rRaman frequency (cm^{-1})			Reference^b
		$\nu_{Fe\text{-}O}$	$\nu_{O\text{-}O}$	ν	
[Fe^{III}(12-TMCO)(Cl)(OO^{t}Bu)]$^+$ (**3**-Cl)	HS	620	830, 873	454	This work
[Fe^{III}(12-TMCO)(Cl)(OOCum)]$^+$ (**3**-Cl’)	HS	624	822, 868	536	This work
[Fe^{III}(6Me$_3$TPA)(OH)(OO^{t}Bu)]$^+$	HS	637	842, 877	-	(S20)
[Fe^{III}(L$_8$Py$_2$)(OTf)(OO^{t}Bu)]$^+$	HS	627	833, 870	-	(S21)
[Fe^{III}(L$_8$Py$_2$)(SAr)(OO^{t}Bu)]$^+$	HS	623	830, 874	-	(S21)
[Fe^{III}(Me$_4$[15]aneN$_4$)(SPh)(OO^{t}Bu)]$^+$	HS	584	843, 872	-	(S22)
[Fe^{III}(Me$_4$[15]aneN$_4$)(OTf)(OO^{t}Bu)]$^+$	HS	612	871	-	(S22)
[Fe^{III}(13-TMC)(OOCum)]$^{2+}$	HS	627	880	-	(S23)
[Fe^{III}(TPA)(OH$_2$)(OO^{t}Bu)]$^{2+}$	LS	696	796	490	(S24)
[Fe^{III}([15]aneN$_4$)(SPh)(OO^{t}Bu)]$^+$	LS	612	795	-	(S25)
[Fe^{III}([15]aneN$_4$)(SPh)(OOCum)]$^+$	L. S.	615	803	-	(S25)
[Fe^{III}(N$_3$PySR)(OO^{t}Bu)]$^{2+}$	L. S.	700	796	-	(S26)

^{a}TPA = tris(2-pyridylmethyl)amine; L$_8$Py$_2$ = N,N-bis(2-pyridylmethyl)-1,5-diazacyclooctane; [15]aneN$_4$ = 1,4,8,12-tetraazacyclopentadecane; 13-TMC = 1,4,7,10-tetramethyl-1,4,7,10-tetraazacyclotridecane. ^{b} Taken from the reported references.

Table S6. Comparison of important bond distances as determined experimentally by Fe K-edge EXAFS and theoretically from DFT of **3**-Cl

Bond	**Distance from EXAFS (Å)**	**Distance from DFT (Å)**
Fe-O (OO^{t}Bu)	1.82	1.89
Fe-O (ligand)	2.04	2.22
Fe-Cl (*cis*-ligand)	2.26	2.28
Fe-N (avg)	2.19	2.26

Table S7. Comparison of the absorbance maxima (λ_{max}) and molar extinction coefficient of **3**-L′ intermediate with different anionic ligands determined from UV-vis spectral analysis

Additive (L′)	λ_{max} **(nm)**	ε **(M^{-1} cm^{-1})**
$MePhS^-$	460	607
F^-	506	637
Cl^-	517	880
Br^-	538	837

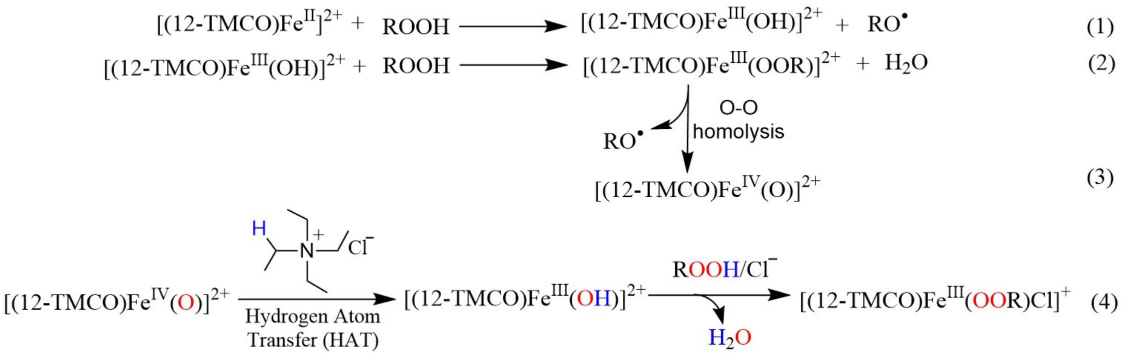
[(12-TMCO)Fe^II]^2+ + ROOH → [(12-TMCO)Fe^III(OH)]^2+ + RO•
(1)
[(12-TMCO)Fe^III(OH)]^2+ + ROOH → [(12-TMCO)Fe^III(OOR)]^2+ + H2O
(2)
O-O
homolysis
RO•
[(12-TMCO)Fe^IV(O)]^2+
(3)
H
N
+
Cl⁻
[(12-TMCO)Fe^IV(O)]^2+
Hydrogen Atom
Transfer (HAT)
[(12-TMCO)Fe^III(OH)]^2+
ROOH/Cl⁻
H2O
[(12-TMCO)Fe^III(OOR)Cl]^+
(4)

Scheme S1

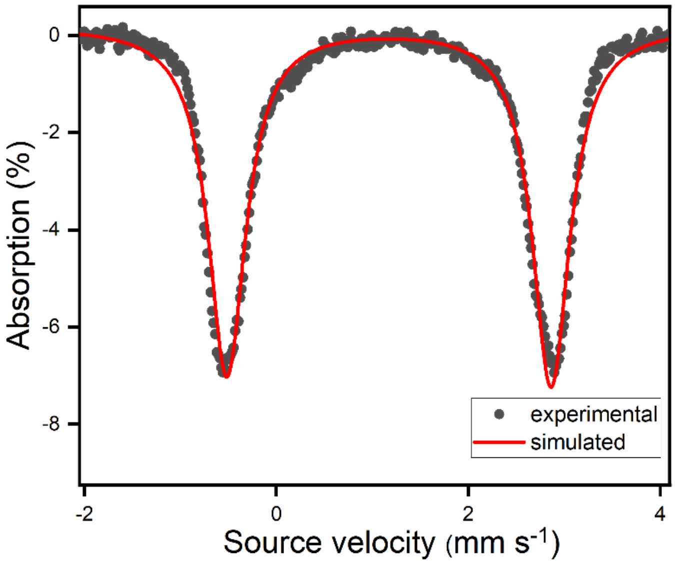

Fig. S1 Zero-field Mössbauer spectrum of complex **1-**(OTf)$_2$ with isomer shift, δ = 1.17 mm s^{-1} and quadrupole splitting, ΔE_Q = 3.38 mm s^{-1} recorded at 4.2 K.

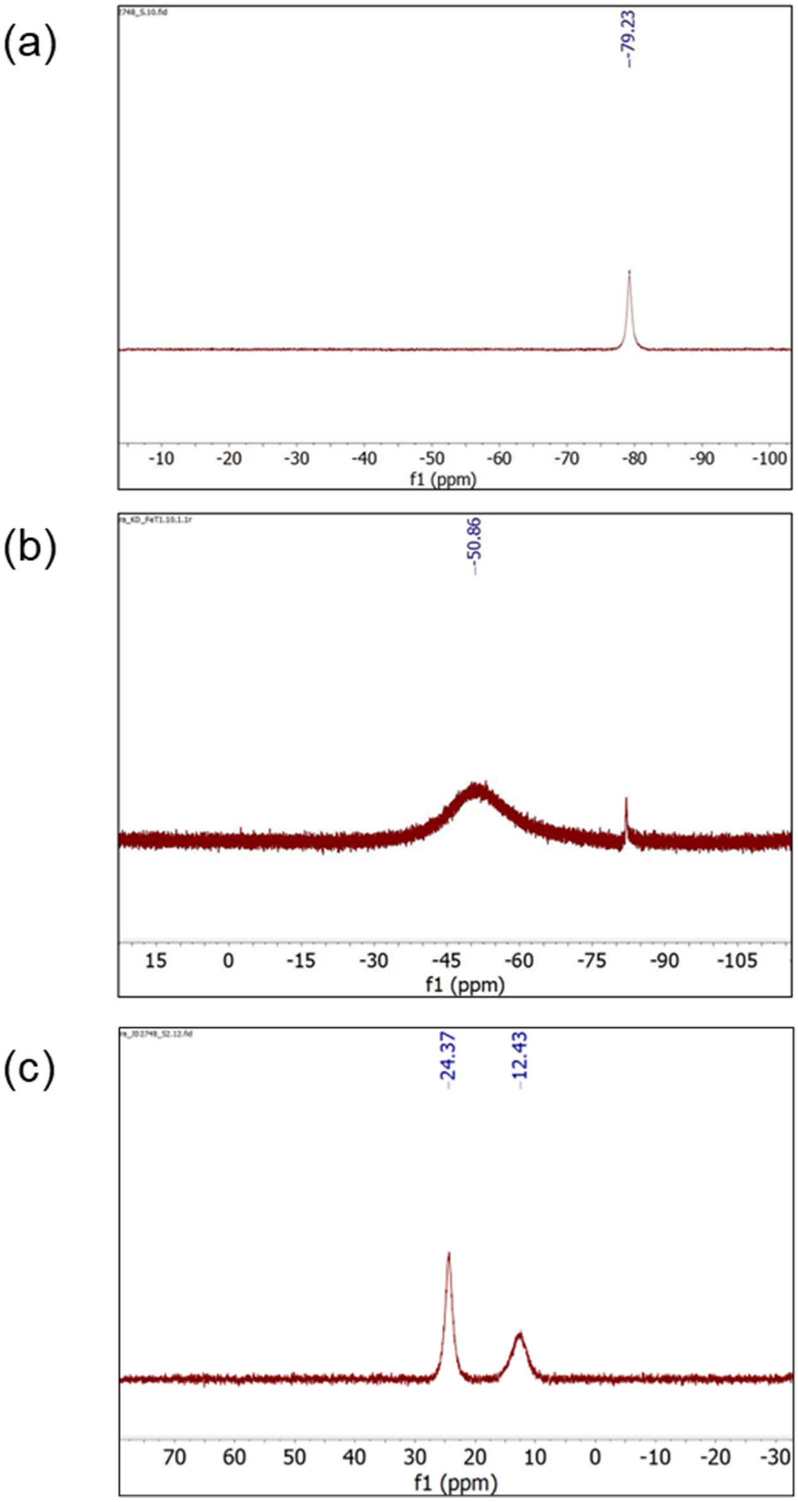

Fig. S2 ^{19}F NMR spectra of complex **1**-(OTf)$_2$ in (a) CH$_3$CN-*d*$_3$ and (b) acetone-*d*$_6$, and (c) ^{1}H NMR spectrum of **1**-(OTf)$_2$ in) CH$_3$CN-*d*$_3$ recorded in 300 MHz.

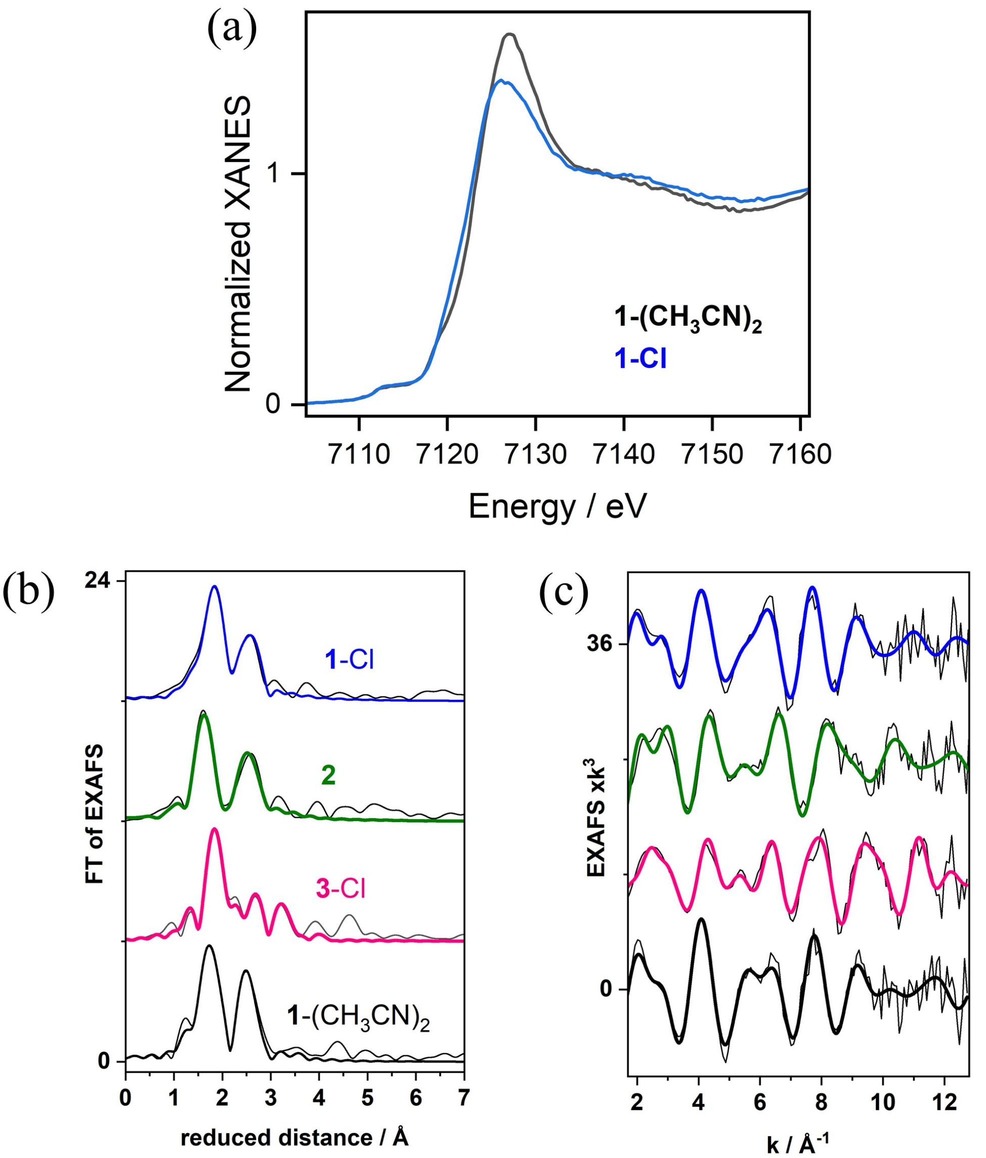

Fig. S3 (a) Fe K-edge XANES spectra of the solutions **1**-(CH_3CN)$_2$ (black) and **1**-Cl (blue). (b) Fourier-transformed (FT) Fe K-edge EXAFS data of the solutions **1**-(CH_3CN)$_2$ (black), **1**-Cl (blue), **2** (green) and **3**-Cl (pink) in CH_3CN (thin black lines: experimental spectra, thick colored lines: simulated spectra). (c) The k^3-weighted EXAFS spectra on a wavevector (k) scale (**1**-(CH_3CN)$_2$ (black), **1**-Cl (blue), **2** (green) and **3**-Cl (pink); thin black lines: experimental spectra, thick colored lines: simulated spectra with parameters in **Table S2**).

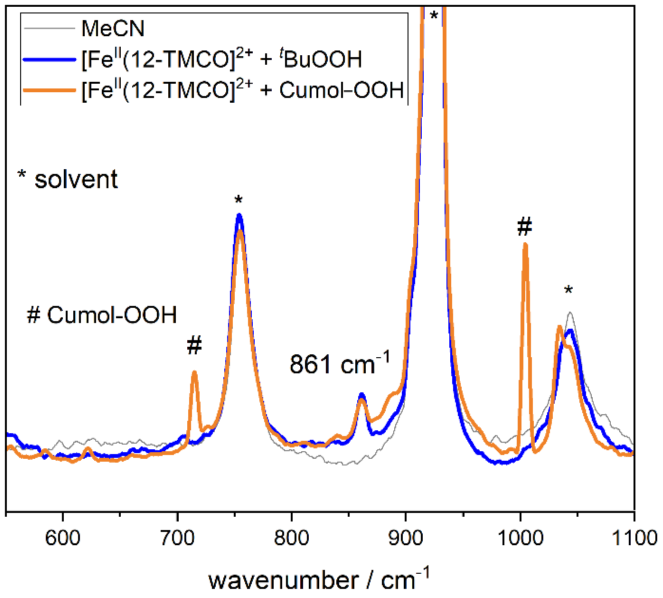

Fig. S4 rRaman spectra of species **2** generated in the reaction of **1**-(CH_3CN)$_2$ (4 mM) with 20 equiv. (a) ^{t}BuOOH (blue) and (b) CumOOH (orange) in CH_3CN at -40°C using 406 nm laser excitation.

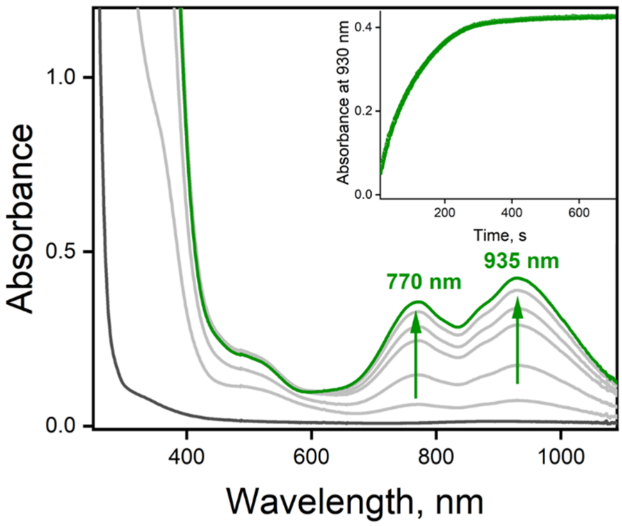

Fig. S5 UV-vis spectral changes observed in the reaction of **1**-(CH_3CN)$_2$ (4 mM) (black) upon addition of cumenehydroperoxide (CumOOH, 20 equiv.) in CH_3CN at -20°C. Inset shows the time profile for the generation of the peak at 935 nm corresponding to **2**.

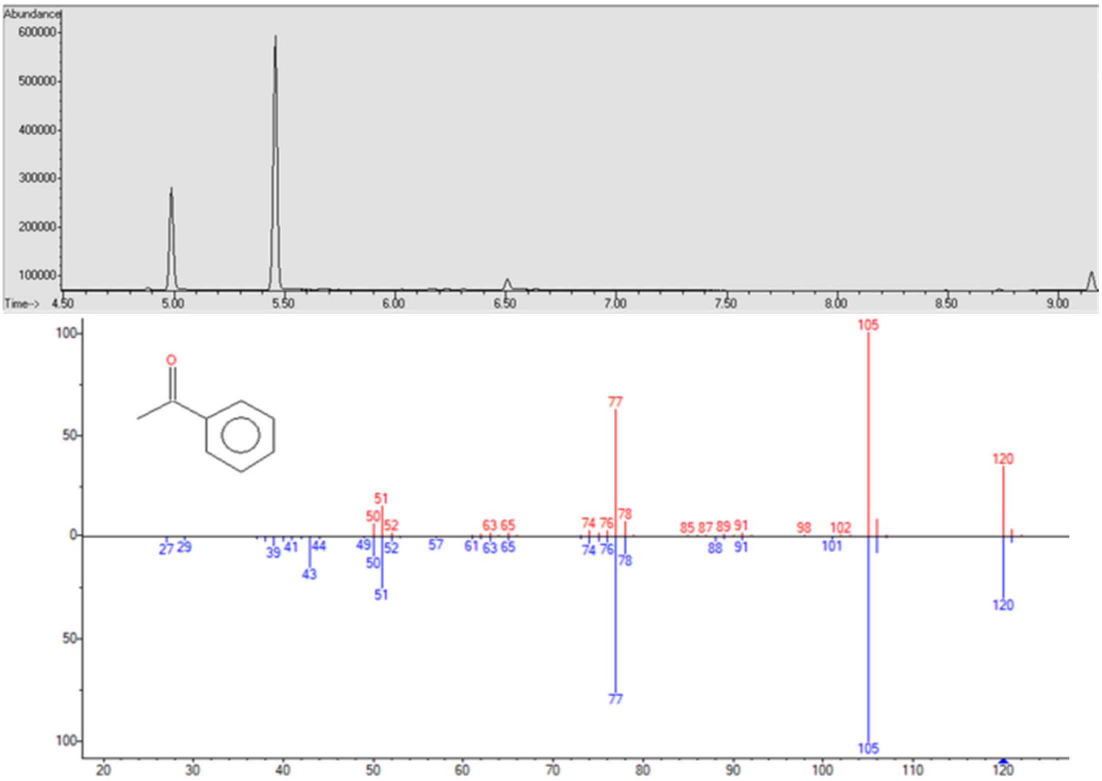

Fig. S6 GC-MS analysis of the organic product after reaction of a 4 mM solution of complex **1**-(CH$_3$CN)$_2$ in CH$_3$CN with 20 equiv. of CumOOH at -20°C. The formation of acetophenone is detected at 4.98 minutes by comparing with standard and also confirmed through bibliographic data. The yield was determined to be 96% with respect to known concentration of biphenyl (1mM, 9.15 min).

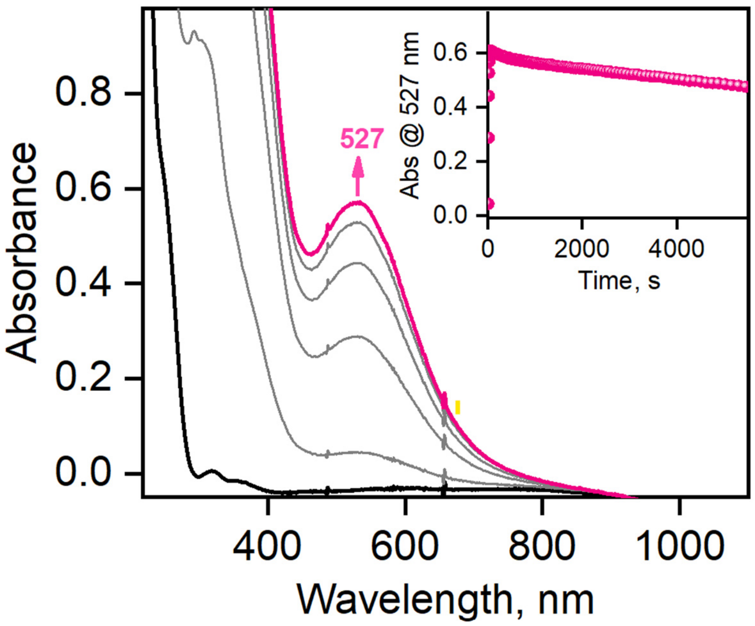

Fig. S7 UV-vis spectral changes observed upon addition of ^{t}BuOOH (20 equiv. pink line) to **1**-Cl (0.5 mM, black line) in CH_3CN at -20°C. Inset shows the natural decay of the species at 527 nm.

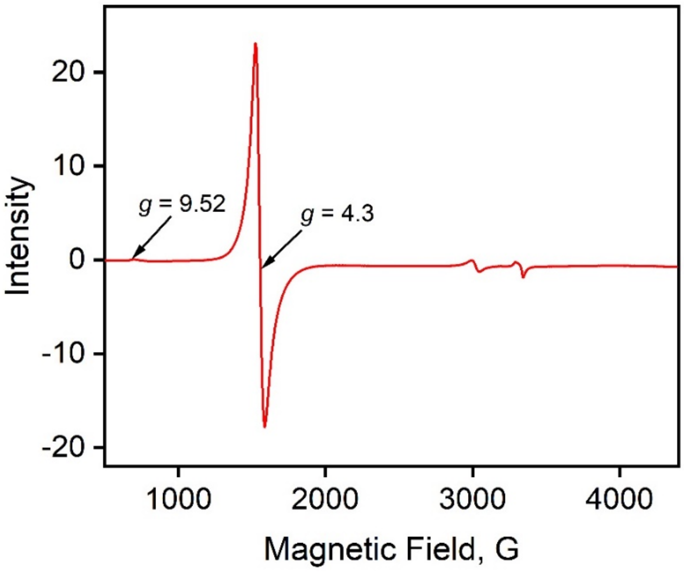

Fig. S8 The CW X-band EPR spectrum of **3**-Cl showing EPR active signals at *g* = 9.52, and 4.3 corresponding to a high-spin iron(III) (*S* = 5/2) center. The sample was recorded in CH_3CN at recorded at 13 K.

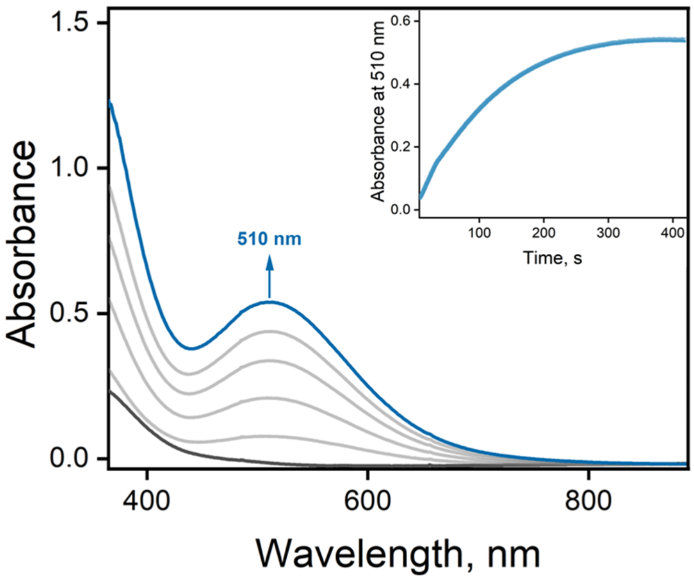

Fig. S9 UV-vis spectral changes observed in the reaction of **1**-(OTf)$_2$ (black) with ^{t}BuOOH (20 equiv.) due to the generation of **3-**OTf (blue) in acetone at -40°C. Inset shows the time profile for the generation of the peak at 510 nm.

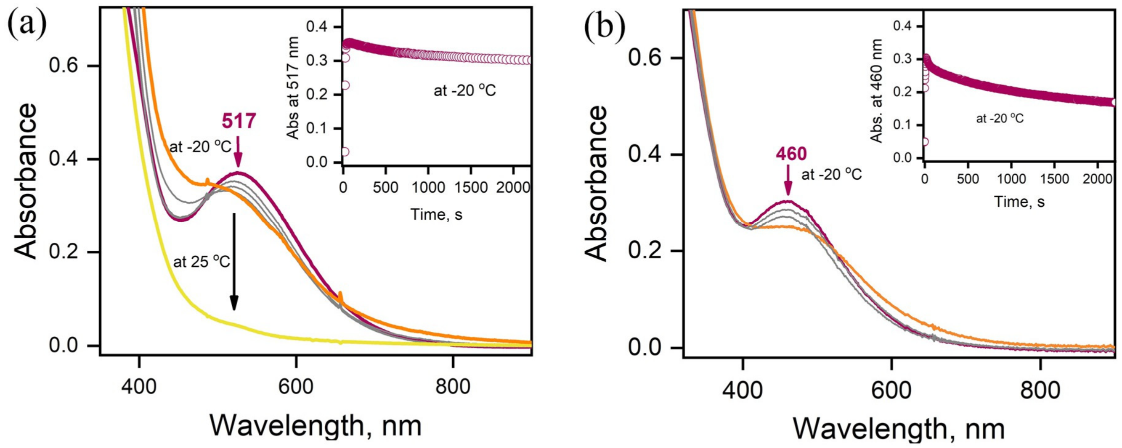

Fig. S10 UV-vis spectral changes observed in the natural decay of **3**-Cl (a) and **3**-SPhMe (b) at -20 ºC. Inset shows the time profile for the decay of **3**-Cl at 517 nm (a) and **3**-SPhMe at 460 nm (b) monitored at -20 ºC in CH_3CN.

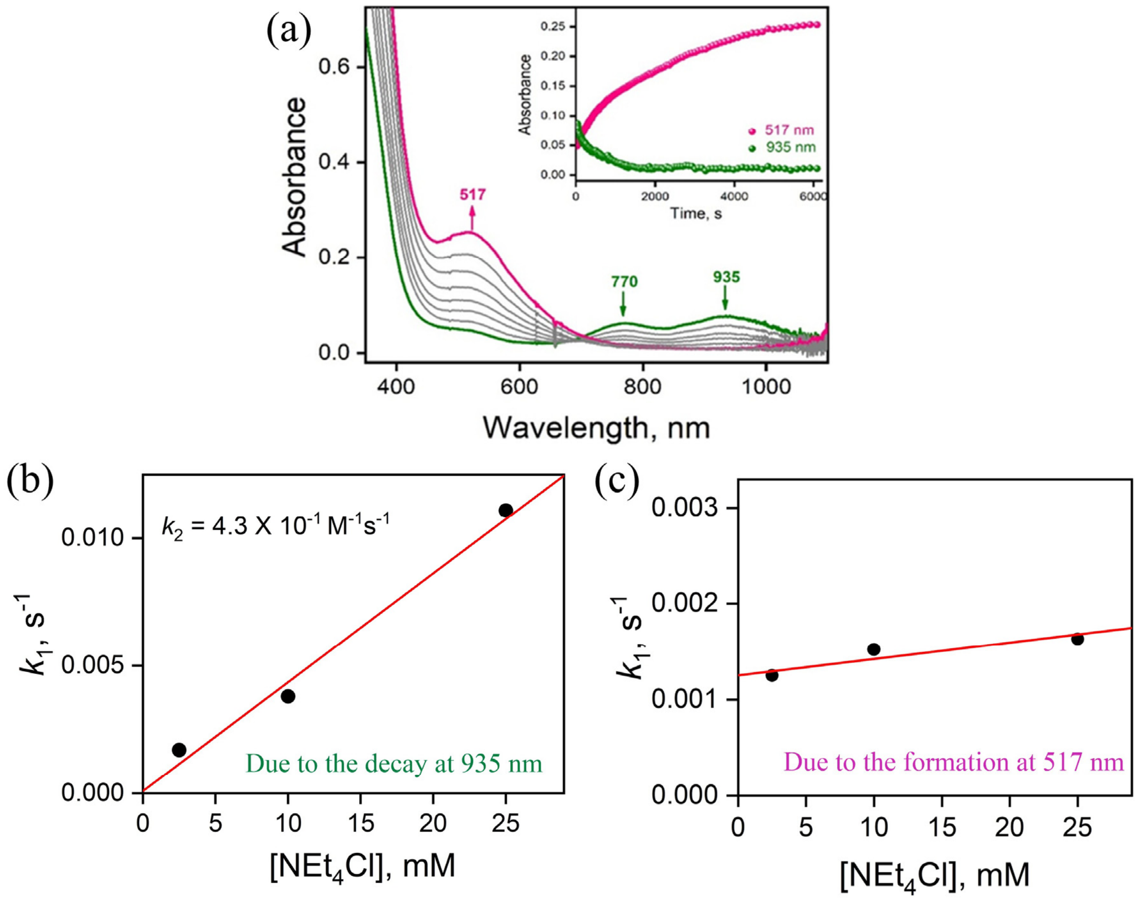

Fig. S11 (a) UV-vis spectral changes observed due to the decay of **2** (green) and the concomitant generation of **3**-Cl (pink) after the reaction of **2** (0.5 mM, cell path length = 0.5 cm) with NEt_4Cl (5 equiv.) in the presence of excess ^{t}BuOOH in CH_3CN at -20 ºC. Inset shows the time profile for the decay of **2** at 935 nm and for the generation of **3**-Cl at 517 nm. (b) Plot of pseudo-first order rate constant (k_1) vs. different concentration of NEt_4Cl for the decay of **2** in CH_3CN at -20 ºC. (c) Plot of pseudo-first order rate constant (k_1) vs. different concentration of NEt_4Cl for the formation of **3-**Cl in CH_3CN at -20 ºC.

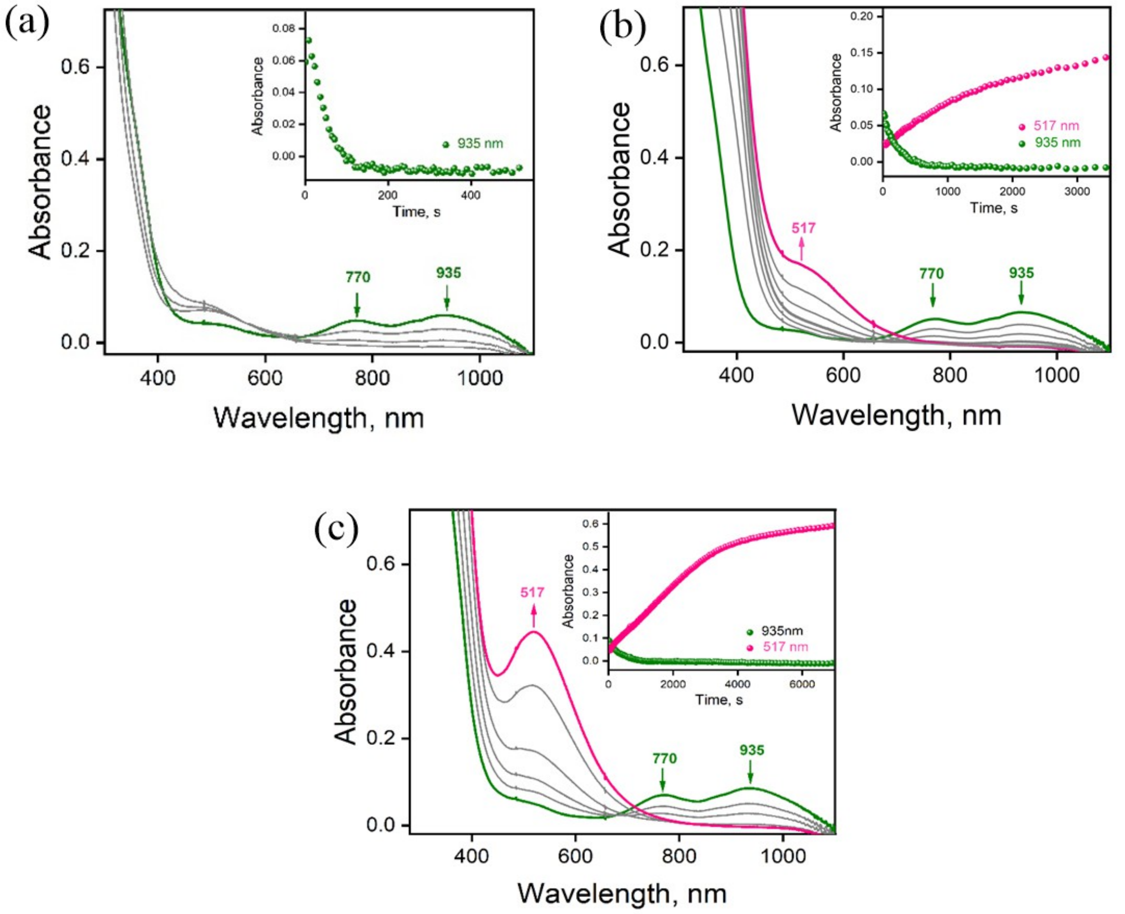

Fig. S12 UV-vis spectral changes observed due to the decay of **2** (0.5 mM) in the presence of different anionic ligands (a) F^- (NMe_4F, 5 equiv.), (b) Br^- (NEt_4Br, 5 equiv.), and (c) Cl^- (NEt_4Cl, 5 equiv.) in CH_3CN at – 20 °C. Inset shows the decay of **2** at 935 nm (green line).

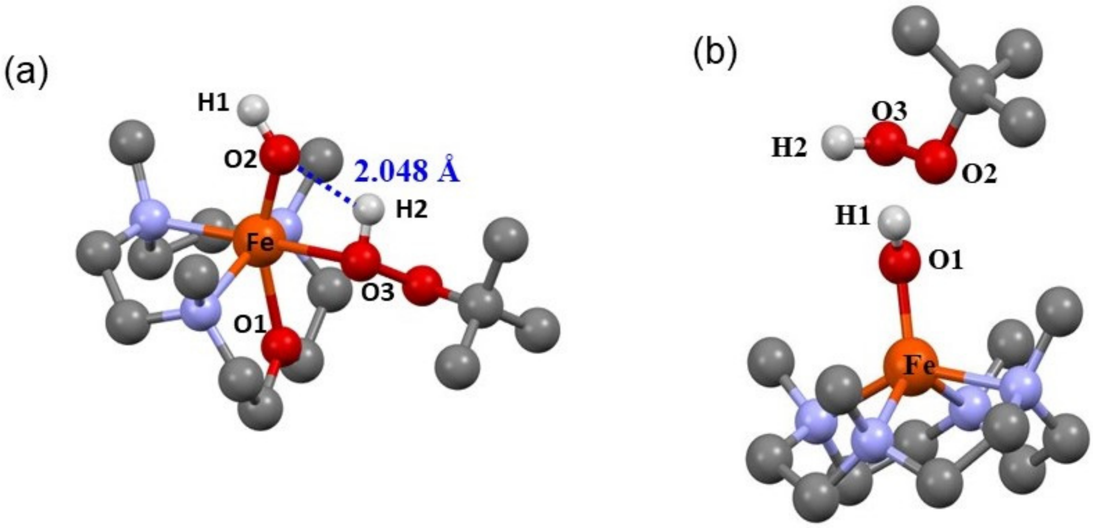

Fig. S13 (a) DFT optimized structure of $[Fe^{III}(12\text{-}TMC)(OH)(^{t}BuOOH)]^{2+}$ (**5**) presumably stabilized by H-bonding interaction. (b) DFT optimized structure showing the non-coordinated ^{t}BuOOH group with $[Fe^{III}(12\text{-}TMC)OH]^{2+}$. H-atoms associated with carbon atoms are removed for clarity.

NMR data for the 12-TMCO ligand

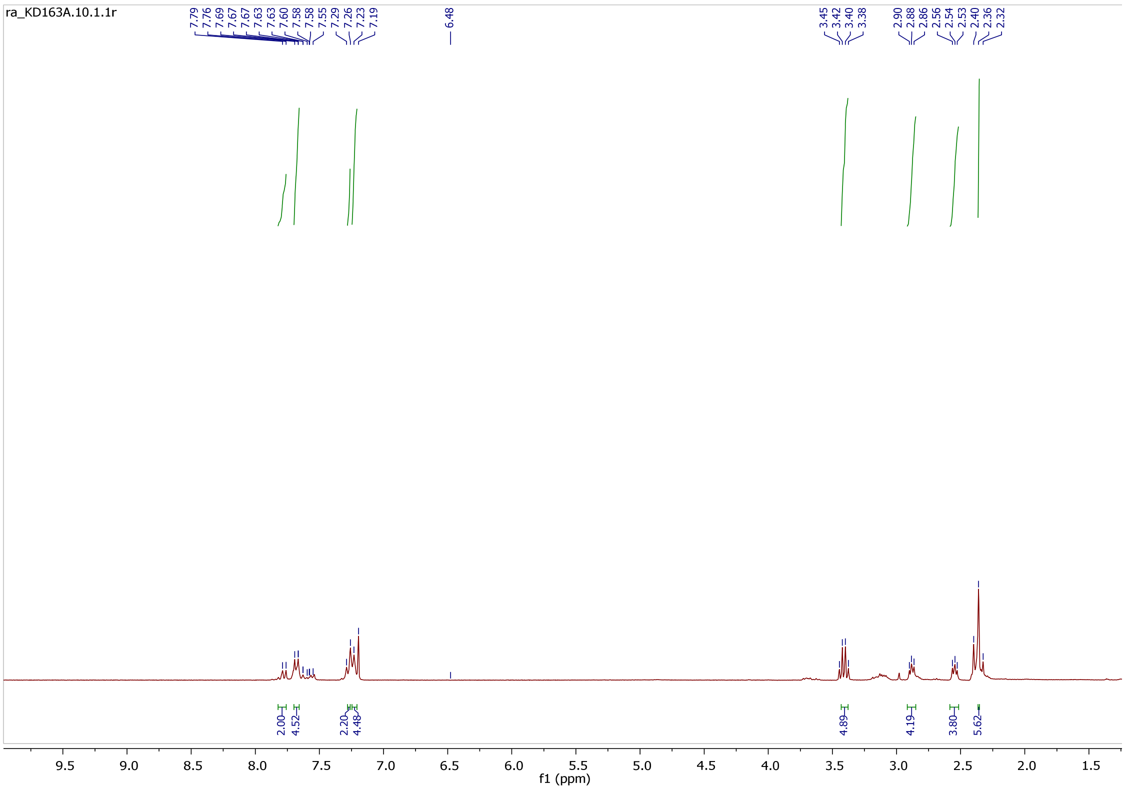

Fig. S14 ^{1}H NMR spectrum of *N,N',N''*-tritosylbis(2-aminoethyl)amine in CDCl$_3$ at 300 MHz.

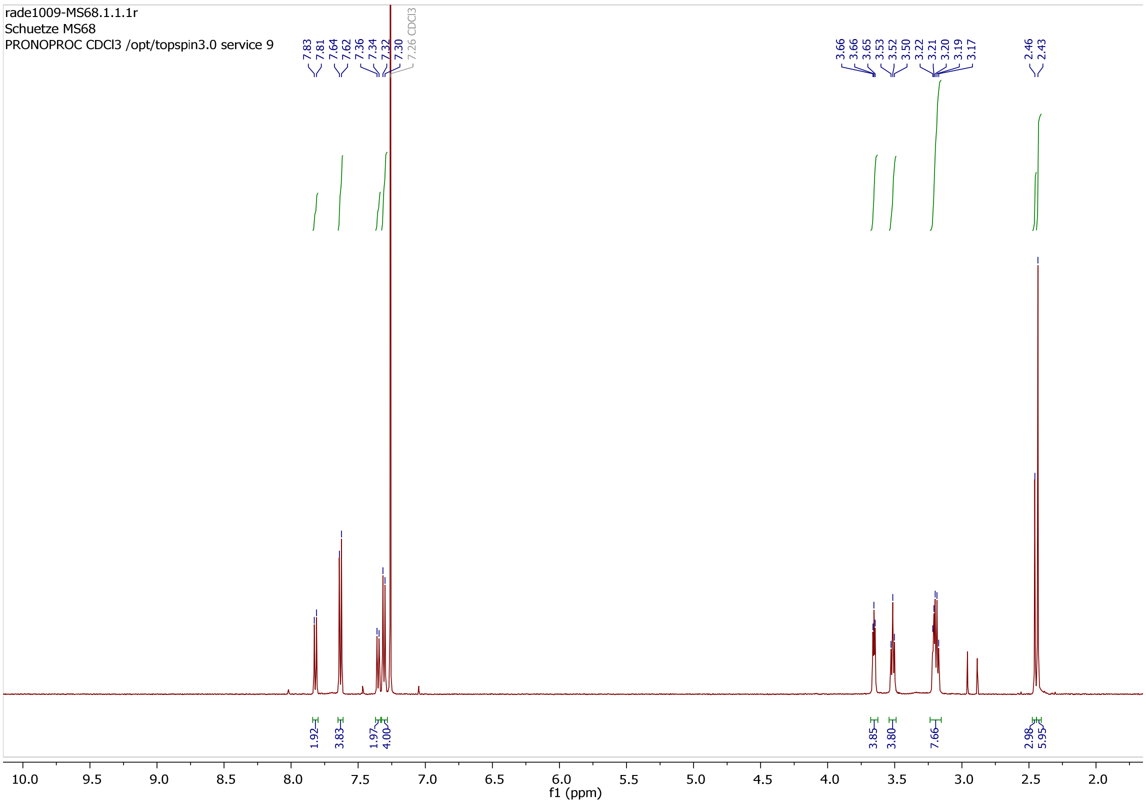

Fig. S15 ^{1}H NMR spectrum of 4,7,10-Tritosyl-1-oxa-4,7,10-triazacyclododecane in $CDCl_3$ at 300 MHz.

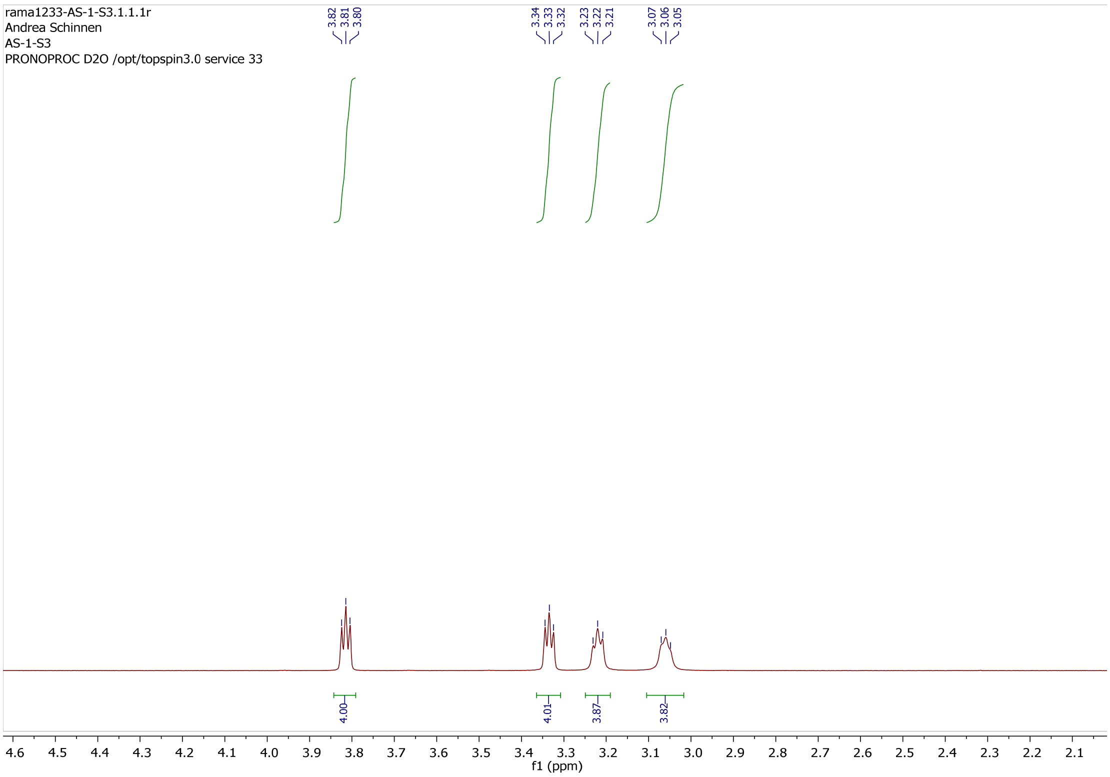

Fig. S16 ^{1}H NMR spectrum of 1-oxa-4,7,10-triazacyclododecane in D_2O at 300 MHz.

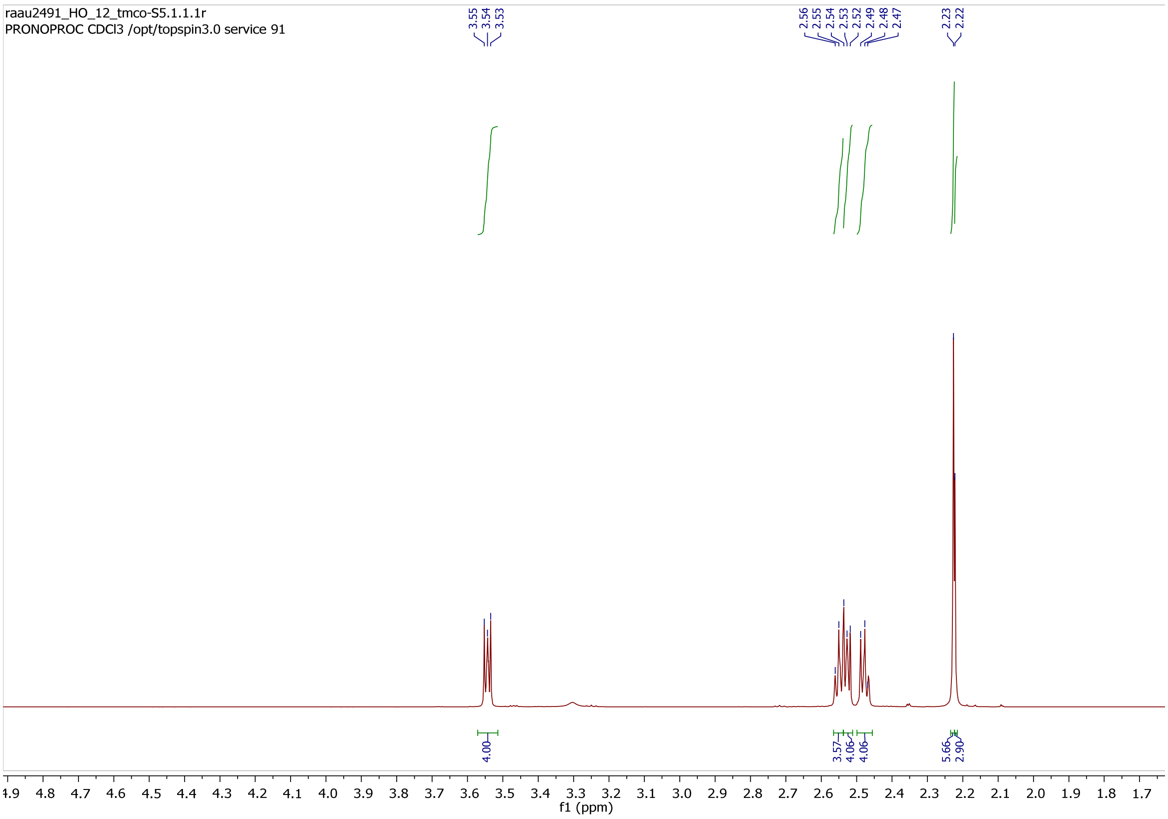

Fig. S17 ^{1}H NMR spectrum of 4,7,10-trimethyl-1-oxa-4,7,10- triazacyclotedodecane in $CDCl_3$ at 300 MHz.

NMR data for the 12-TMC ligand

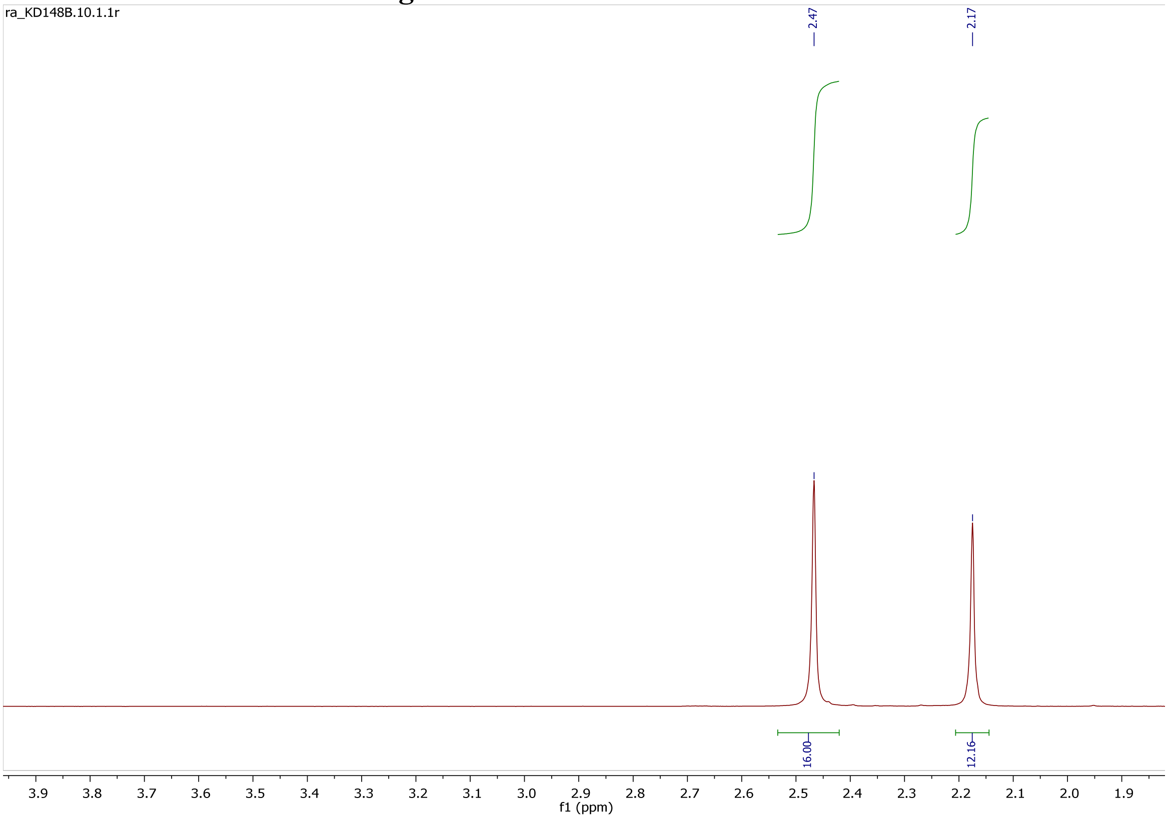

Fig. S18 ^{1}H NMR spectrum of 1,4,7,10-tetramethyl-1,4,7,10-tetraazacyclotedodecane in $CDCl_3$ at 300 MHz.